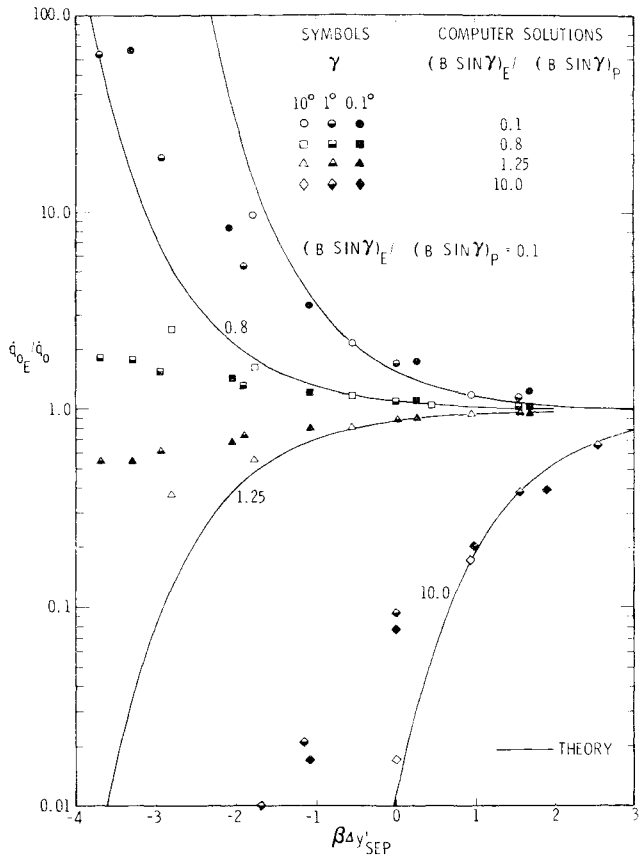

Fig. 5 Comparison of heating rate ratios.

Case 1: If $B_E \sin\gamma_E = B_P \sin\gamma_P$, then $\mathbf{V}_E$, $\mathbf{a}_E$, and $\dot{q}_{0E}$ are the same as would be experienced on a nonstaged trajectory for the same $B \sin\gamma$.

Case 2: If $B_E \sin\gamma_E > B_P \sin\gamma_P$, then $\mathbf{V}_E$, $\mathbf{a}_E$, and $\dot{q}_{0E}$ are less than would be experienced on a nonstaged trajectory for the same $B \sin\gamma$ ($= B_E \sin\gamma_E$).

Case 3: If $B_E \sin\gamma_E < B_P \sin\gamma_P$, then $\mathbf{V}_E$, $\mathbf{a}_E$, and $\dot{q}_{0E}$ are greater than would be experienced on a nonstaged trajectory for the same $B \sin\gamma$ ($= B_E \sin\gamma_E$).

These relations are illustrated graphically in Fig. 3 for typical re-entry behavior. The solid lines represent the nonstaged trajectory for $B \sin\gamma = B_E \sin\gamma_E$ (case 1). The long-dashed curves represent case 2; the short dashed curves, case 3. Points A and B, for cases 2 and 3, respectively, represent situations where separation occurs before the altitude of peak deceleration or peak heating rate for the ejected body is reached; i.e., $\mathbf{a}_{E\max}$ and $\dot{q}_{0E\max}$ are experienced following release. Points C and D represent the similar situations where y_{sep} is below the computed altitude of peak deceleration or peak heating rate for the ejected body. In this event, $\mathbf{a}_E$ and $\dot{q}_{0E}$ decrease monotonically with time following release.

Figures 4 and 5 compare these theoretical approximations (the curves) with solutions (points for y_{sep}) provided by a digital program[5] (which numerically integrates the complete equations of motion) for $V_I = 24{,}000$ fps and for $(B \sin\gamma)_E/(B \sin\gamma)_P = 10$, 1.25, 0.8, and 0.1. Separation altitudes investigated spanned the range from above the peak heating rate to below peak deceleration. For each value of $(B \sin\gamma)_E/(B \sin\gamma)_P$, computer trajectory solutions were calculated for γ_I's of 10°, 1° and 0.1° to cover the range from steep ballistic or launch abort re-entry to shallow orbital decay reentry. Whereas the approximate theory indicates that the $\mathbf{V}$, $\mathbf{a}$ and $\dot{q}_0$ ratios are constant following separation, the computer solutions indicate that the ratios tend to approach unity with increasing time following separation. The approximate theory does, however, provide a good correlation of the ratios at y_{sep}, and it quite adequately indicates the influences of the various parameters involved. It is apparent that the influence of the staging process on the velocity, deceleration, and stagnation point heating rate increases as separation is delayed along the trajectory (i.e., as Δy_{sep} decreases to negative values) or as the disparity in $B \sin\gamma$ values for the ejected and parent bodies increases.

References

[1] Allen, H. J. and Eggers, A. J., Jr., "A Study of the Motion and Aerodynamic Heating of Ballistic Missiles Entering the Earth's Atmosphere at High Supersonic Speeds," Rept. 1381, 1958, NACA.

[2] *U.S. Standard Atmosphere*, 1962, Superintendent of Documents, U.S. Government Printing Office, Washington 25, D.C.

[3] Kemp, N. H. and Riddell, F. R., "Heat Transfer to Satellite Vehicles Re-entering the Atmosphere," *Jet Propulsion*, Vol. 27, No. 2, Feb. 1957, pp. 132–137.

[4] Detra, R. W., Kemp, N. H., and Riddell, F. R., "Addendum to Heat Transfer to Satellite Vehicles Re-entering the Atmosphere," *Jet Propulsion*, Vol. 27, No. 12, Dec. 1957, pp. 1256–1257.

[5] Allensworth, J. A. F., "The TTA Generalized Rigid Body Trajectory Program for Digital Computer," SC-DR-65-511, Aug. 1966, Sandia Labs., Albuquerque, N. Mex.

Radiation Heat Transfer Around the Interior of a Long Cylinder

JOHN D. GRAHAM*

Spar Aerospace Products, Malton, Ontario, Canada

Nomenclature

A,A_1	=	area elements on cylinder surface
B,F,H	=	$B(\theta),F(\theta),H(\theta)$, Eqs. (6, and 8), respectively
b,b_1	=	one half length of longitudinal area elements
C,D	=	solution constants, see Eq. (11)
E	=	emissive power
l_1	=	see Ref. 3
q_0	=	net heat loss at position zero
r	=	cylinder radius
T_θ	=	temperature at position θ
ϵ	=	interior surface emissivity to (and absorptivity for) infrared radiation
θ	=	position around cylinder (see Fig. 1)
σ	=	Stefan-Boltzmann constant
ϕ,ϕ_1	=	see Ref. 3

Introduction

THERE is presented the derivation of a simple expression for the radiation heat transfer around the interior of a long cylinder in terms of the emissivity ϵ of the surface. It is assumed that ϵ is constant over the entire surface and that all reflections are diffuse. Also, the temperature distribution is assumed independent of length.

One of the immediate applications for this result is in determining radiant heat transfer in STEMs.[1] Often in the thermal analysis of conventional STEMs the radiant heat transfer can be neglected, as it is small compared to conduction around the metallic cross section. However, some recent STEM concepts[2] have an overlapping type contact across which the conduction is poor, thus necessitating the consideration of radiation heat transfer.

Specifically we will find an expression for $B(\theta)$ which is the proportion of radiation emitted from a longitudinal area element at position θ on the cylinder interior (Fig. 1) which,

Received July 23, 1969; revision received December 22, 1969. The support for this work was provided in part by D.I.R. Grant 5540/33 from the Defense Research Board of Canada.

* Head, Systems Analysis. Member AIAA.

after any number of reflections around the interior, is eventually absorbed at a similar area element at position zero. With the emitting power at any section θ given by $E_\theta = \epsilon\sigma T_\theta^4$, the expression for $B(\theta)$ can be used to give the net heat loss at an area element, viz.,

$$q_0 = \epsilon\sigma\left[T_0^4 - \int_0^{2\pi} B(\theta)T_\theta^4 d\theta\right] \quad (1)$$

Analysis

First, there will be determined the shape factor[3] between two narrow longitudinal area elements separated by an angle θ, one of length $2b_1$ and area $A_1 = 2b_1 r\delta\theta_1$, the other of length $2b$ and area $A = 2br\delta\theta$ (see Fig. 1). The elements are symmetrically placed about the same section of the cylinder. The shape factor between any two infinite simal lengths of these areas, respectively of area dA_1 and dA is given by[3]

$$dA_1F_{dA_1\to dA} = (\cos\phi_1 \cos\phi dA_1 dA)/l_1^2 \quad (2)$$

Integrating over the total lengths $2b_1$ and $2b$ it is found from geometrical considerations that the shape factor between areas A_1 and A is given by

$$A_1F_{A_1\to A} = (1/\pi)d\theta_1 d\theta(1 - \cos\theta)^2$$
$$\int_{-b}^{b}\int_{-b_1}^{b_1}\left\{1\Big/\left[2(1 - \cos\theta) + \left(\frac{z_1 - z}{r}\right)^2\right]^2\right\} dz_1 dz =$$
$$(1/2\pi)d\theta_1 d\theta r \sin^2\frac{\theta}{2}\left[(b_1 + b)\tan^{-1} b_1 + b\Big/2r\sin\frac{\theta}{2} - (b - b_1)\tan^{-1} b - b_1\Big/2r\sin\frac{\theta}{2}\right] \quad (3)$$

For the special case of area elements of the same length $2b$ in which we are interested, Eq. (3) reduces to, after division by $A_1 = 2brd\theta$,

$$F_{A_1\to A} = \{\sin(\theta/2)\tan^{-1}[b/r\sin(\theta/2)]/2\pi\}d\theta \quad (4)$$

At this stage we introduce the distribution $F(\theta)$ which defines the distribution function for radiation leaving a longitudinal area element at section θ and incident on a longitudinal area element at section zero. Then $F(\theta)$ equals the quantity in braces in Eq. (4). In the limit of a very long cylinder $b \to \infty$ and†

$$F(\theta) = \tfrac{1}{4}\sin\theta/2 \quad (5)$$

To determine $B(\theta)$ there is required the proportion of radiation directly radiated from θ and absorbed at zero together with that which is reflected about the interior and is eventually absorbed at zero. The proportion directly emitted from θ and absorbed at zero is given by $\epsilon F(\theta)$. For a general section at ψ, the proportion incident from θ is given by $F(|\psi - \theta|)$, and then $(1 - \epsilon)$ of this amount is diffusely reflected around the interior. This reflected radiation will itself be absorbed at various points around the interior in a similar manner to that radiation which is directly emitted from ψ. Integrating over all such sections ψ, we can find

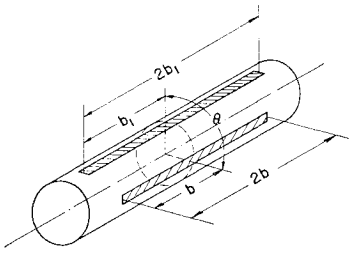

Fig. 1 Internal longitudinal area elements separated by θ.

† This result was obtained previous to the author by K. Farrell of RCA Ltd., Montreal (previously with Spar Aerospace Products, Ltd.).

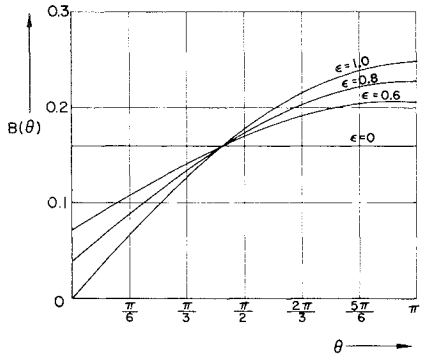

Fig. 2 $B(\theta)$ as a function of θ and ϵ.

$B(\theta)$, which is defined as the proportion of radiation emitted from θ and eventually absorbed at zero‡

$$B(\theta) = \epsilon F(\theta) + (1 - \epsilon)\int_0^{2\pi} F(|\psi - \theta|)B(\psi)d\psi \quad (6)$$

Substituting from (5) gives

$$B(\theta) = \epsilon/4\sin\theta/2 + 1/4(1 - \epsilon)H(\theta) \quad (7)$$

where

$$H(\theta) = \int_0^\theta B(\psi)\sin(\theta - \psi)/2d\psi + \int_\theta^{2\pi} B(\psi)\sin(\psi - \theta)/2d\psi \quad (8)$$

Differentiating (7) twice with respect to θ leads to

$$d^2B(\theta)/d\theta^2 = -(\epsilon/16)\sin\theta/2 + (1 - \epsilon)B(\theta)/4 - (1 - \epsilon)H(\theta)/16 \quad (9)$$

Eliminating $H(\theta)$ between Eqs. (7) and (9) leads to

$$d^2B(\theta)/d\theta^2 + (\epsilon/4)B(\theta) = 0 \quad (10)$$

which has a solution of the form

$$B(\theta) = D\sin\epsilon^{1/2}\theta/2 + C\cos\epsilon^{1/2}\theta/2 \quad (11)$$

where D and C are, as yet, unknown.

Substitution of Eq. (11) into (6) leads, after much manipulation, to

$$\sin\theta/2[\epsilon/4 + D\epsilon^{1/2}(\cos\epsilon^{1/2}\pi - 1)/2 - C\epsilon^{1/2}(\sin\epsilon^{1/2}\pi - 1)/2] \quad (12)$$

$$+ \cos\theta/2[(D\epsilon^{1/2}\sin\epsilon^{1/2}\pi)/2 + C(\cos\epsilon^{1/2}\pi - 1)/2] = 0 \quad (13)$$

Since (13) is valid for all θ then the coefficients of $\sin\theta/2$ and $\cos\theta/2$ must be equal to zero. This leads to

$$D = \epsilon^{1/2}/4,\ C = \epsilon^{1/2}\sin\epsilon^{1/2}\pi/4(1 - \cos\epsilon^{1/2}\pi) \quad (14)$$

Substituting (14) in (11), there is obtained after some manipulation

$$B(\theta) = \epsilon^{1/2}\cos[\epsilon^{1/2}(\pi - \theta)/2]/4\sin(\epsilon^{1/2}\pi/2) \quad (15)$$

which is a relatively simple expression.

For the limiting case when $\epsilon = 1$ (i.e., zero reflectivity) it reduces to the shape factor as expected

$$B(\theta) = \tfrac{1}{4}\sin\theta/2 = F(\theta) \quad (16)$$

$B(\theta)$ is plotted as a function of θ in Fig. 2 for different values of ϵ. As would be expected the higher the value of ϵ the higher is the proportion of heat transferred from the hot to the cold side of the cylinder. In the limit as $\epsilon \to 0$ it can be shown from (15) that $B(\theta) \to \frac{1}{2}\pi$ which is inde-

‡ This argument has been used in Ref. 3 for discrete area elements to generate a set of simultaneous linear equations.

pendent of θ, indicating an equal distribution of emitted radiation.

References

[1] MacNaughton, J. D., "Unfurlable Metal Structures for Spacecraft," *Canadian Aeronautics and Space Journal*, Vol. 9, No. 4, 1963, pp. 103–116.

[2] Grimshaw, E. R. and Wells, A., "Gravity Gradient Booms—Their Origin and Evolution," Dec., 1968, Symposium on Gravity Gradient Attitude Control, Sponsored by the Air Force (SAMSO) and Aerospace Corporation, Los Angeles, Calif.

[3] Kreith, F., "Radiation Heat Transfer," International Textbook, Scranton, Pa., 1962, pp. 40–42, 50–51.

Effect of Reflections from CO_2 Cryodeposits on Thermal Testing in Space Chambers

D. W. Mills Jr.* and A. M. Smith†
ARO Inc., Arnold Air Force Station, Tenn.

In space simulators the test vehicle is surrounded by black surfaces which are cooled to near 77°K to minimize their emitted radiant flux and to increase the vacuum pumping capacity of the space chamber. If CO_2 or H_2O cryodeposits form on the black cryopanels, their visible and near-infrared reflectance properties are altered.[1] This Note presents the results of an experiment investigating the effect of reflections from CO_2 cryopanel deposits on the steady-state temperatures of a test article irradiated directly by a simulated solar flux of 140 mw/cm².

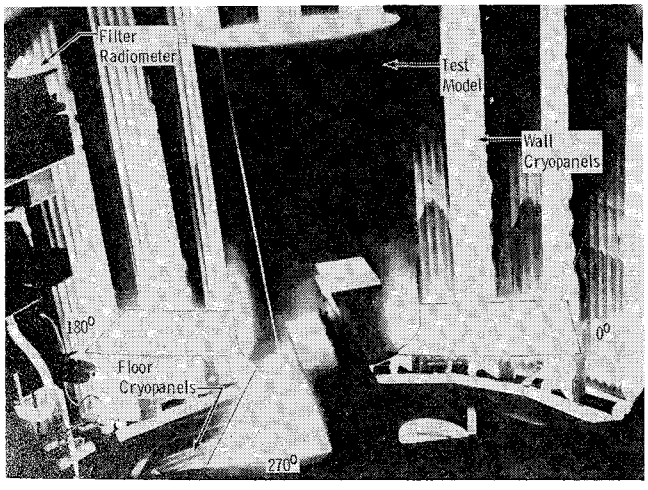

Fig. 1 Hollow cylinder-paddlewheel test model mounted in space simulation chamber showing CO_2 cryodeposits on wall and floor cryopanels.

Presented as Paper 69-1012 at the AIAA/ASTM/IES 4th Space Simulation Conference, Los Angeles, Calif., September 8–10, 1969; submitted October 20, 1969; revision received December 15, 1969. This work was sponsored by the Arnold Engineering Development Center, Air Force Systems Command, under Contract F40600-69-C-0001 with ARO Inc. The tests reported here were carried out in cooperation with the Institut für Raumsimulation, Deutsche Forschungs-und Versuchsanstalt für Luft-und Raumfart, Porz-Wahn, West Germany.

* Research Engineer, Thermal Physics Section, Aerospace Environmental Facility. Associate AIAA.

† Supervisor, Thermal Physics Section, Aerospace Environmental Facility and Associate Professor of Aerospace Engineering (Part-time), University of Tennessee Space Institute, Tullahoma, Tenn. Member AIAA.

The space chamber employed was a vertical cylindrical tank, 12 ft in diameter by 35 ft in height. Its vacuum pumping system consisted of mechanical and oil diffusion pumps, and LN_2-cooled cryopanels. The chamber was equipped with an off-axis, "top sun" solar simulator whose radiation source was an array of 20-kw, short-arc xenon lamps. After passing through an optical integrator, the radiation was reflected downward by a 10-ft-diam collimating mirror to irradiate an 8-ft-diam by 8-ft-deep test volume at one Earth orbit solar constant.

The test article was a closed hollow cylinder with flat paddle surfaces attached to one end (see Fig. 1). This configuration was constructed from 0.125-in.-thick 2024 T4 aluminum sheet and instrumented with copper-constantan thermocouples at the 21 locations shown in Fig. 2. The test model was oriented in the space chamber so that the longitudinal axis of the cylinder was parallel to the collimated beam of solar simulator irradiance. The azimuthal orientation of the model was such that the $\varphi = 270°$ index position (see Figs. 1, 2) faced the chamber viewports. It is seen from Fig. 1 that the top surfaces of the cylinder and paddles, which were irradiated directly by the solar simulator, were coated with white paint. The circumferential surface of the cylinder and the underside of the cylinder and paddles were coated with black paint.

Procedure

The chamber was first evacuated to 10^{-5} torr using mechanical and oil diffusion pumps. Then the cryopanels were cooled with LN_2 thereby surrounding all but the top of the test volume with black 77°K surfaces. After the chamber pressure had decreased to 10^{-6} torr, the solar simulator irradiance was set at 140 mw/cm². The test model was irradiated until its temperatures reached steady-state after 3.1 hr. Readings from the 21 thermocouples on the model were recorded periodically during this time. The solar simulator irradiance was monitored by a filter radiometer (see Fig. 1) and a calibrated thermopile mounted in the chamber at the model level.

After this test run was completed, the solar simulator was turned off and the wall cryopanels were allowed to warm but the floor cryopanels were maintained near 77°K. The conventional pumping system was then valved off and a known quantity of CO_2 was introduced diffusely into the chamber. This formed a given thickness cryodeposit on the floor cryopanels and altered their reflectance. The thickness of CO_2 deposited on the floor cryopanels was determined from

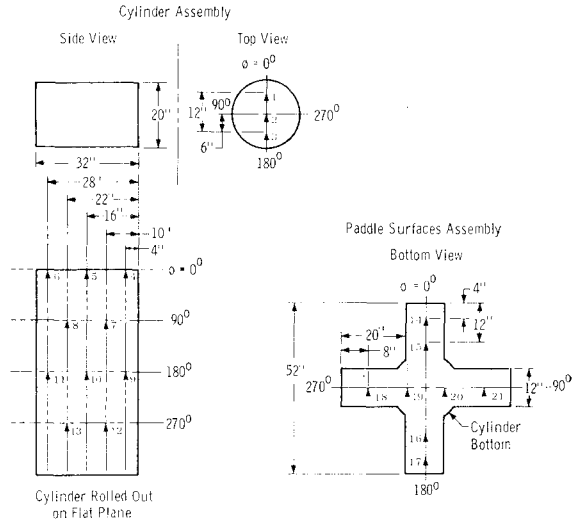

Fig. 2 Thermocouple locations on test model.